

Ferroelectricity of C-Axis Oriented Ba₂NaNb₅O₁₅ on La-doped SrTiO₃ Prepared by Pulsed Laser Deposition

Tohru Higuchi, Minoru Sogawa, Takayuki Kamei and Takeyo Tsukamoto
 Department of Applied Physics, Tokyo University of Science, 1-3 Kagurazaka, Shinjuku, Tokyo 162-8601, Japan
 Fax: 81-3-3260-4772, e-mail: higuchi@rs.kagu.tus.ac.jp

ABSTRACT

Ba₂NaNb₅O₁₅ (BNN) thin films have been prepared on La-doped SrTiO₃ substrates by pulsed laser deposition method. The *c*-axis orientation and surface roughness of the BNN thin films depend on the oxygen gas pressure (*P*_{O₂}) and substrate temperature (*T*_s). When the *P*_{O₂} and *T*_s were fixed at 7.5 mTorr and 700 °C, respectively, the BNN thin film exhibited a highly *c*-axis orientation. The *c*-axis oriented BNN thin film consisted of well-developed grain and exhibited a smooth surface. Then, the remanent polarization (*P*_r) and coercive field (*E*_c) was 2*P*_r=95.3 C/cm² and 2*E*_c=400 kV/cm, respectively.

Key words: Ba₂NaNb₅O₁₅ (BNN), pulsed laser deposition, oxygen gas pressure (*P*_{O₂}), La_{0.05}Sr_{0.95}TiO₃, remanent polarization (*P*_r)

1. INTRODUCTION

Ferroelectric barium sodium niobate, Ba₂NaNb₅O₁₅ (BNN), has a tetragonal tungsten bronze-type structure, which belongs to the point of *mm*2 at room temperature [1-6]. The BNN has two phase transitions above room temperature. One is ferroelectric phase transition at about 560 °C, the other is ferroelastic phase transition at about 300 °C, which is responsible for the formation of twined substructure. The nonlinear optical coefficients are twice as large as those of LiNbO₃ and 20 times higher than those of KH₂PO₄ [7,8]. BNN is resistant to UV irradiation and does not exhibit any optically induced inhomogeneities of the refractive index that occur in LiNbO₃. Furthermore, the spontaneous polarization (*P*_s) and dielectric constant (*ε*) parallel to *c*-axis are 40 μC/cm² and 52, respectively. These large *P*_s and low *ε* are advantageous for application to nonvolatile ferroelectric memories.

The structural and ferroelectric properties of BNN thin films have been reported by Masuda *et al* and co-workers [9-12]. They prepared the random oriented BNN thin films on Pt/Al₂O₃ substrates by rf-magnetron sputtering method. Although the remanent polarization (*P*_r) is approximately 32 μC/cm², the leakage current is very large. In order to prove this problem, they characterized the temperature dependence of the electrical resistivity [10]. The resistivity decreases sharply in the vicinities of 250 and 450 °C. Above 450 °C, the resistivity decreases with increasing temperature, indicating the existence of the conductivity due to oxygen vacancy or Na deficiency at high temperature region.

In this study, the *c*-axis oriented BNN thin films were prepared on La-doped SrTiO₃ (La_{0.05}Sr_{0.95}TiO₃) substrates by pulsed laser deposition (PLD) method. Furthermore, the structural and ferroelectric properties were also characterized. The lattice mismatch between BNN and La_{0.05}Sr_{0.95}TiO₃ was estimated to be

approximately 5.2 % [13-15]. We report in this paper that the delicate controls of substrate temperature (*T*_s) and oxygen gas pressure (*P*_{O₂}) during the deposition are important in order to prepare *c*-axis oriented BNN thin film.

2. EXPERIMENTAL

BNN thin films were deposited on (100)-oriented La_{0.05}Sr_{0.95}TiO₃ substrate by PLD method using BNN ceramic target. The La_{0.05}Sr_{0.95}TiO₃ substrates, which were grown by the Czochralski method, were obtained from Earth Jewelry Co. Ltd. The BNN ceramic target was prepared as follows. BaCO₃, NaCO₃ and Nb₂O₅ powders were mixed with cation molar ratio of Ba:Na:Nb=2:1:5 using a wet ball mill. The mixture was pressed into a disk shape at 4.9 kg/cm² and sintered for 6h at 1350°C. The target disk was polished to 21.5 mm diameter and 4 mm thickness. The prepared BNN ceramic target was examined using XRD, as shown in Fig.1.

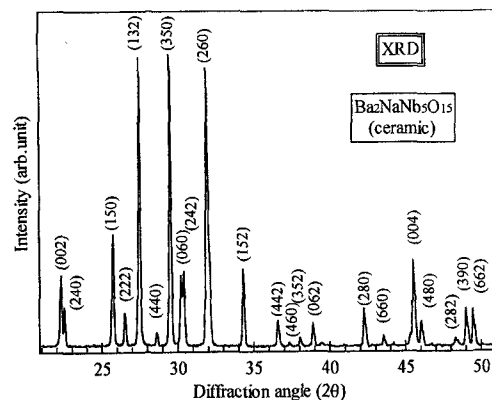


Fig. 1 XRD pattern of BNN ceramics.

The PLD system was arranged in a symmetric configuration with a rotating substrate holder for compositional uniformity. The base pressure was ordinarily 2×10^{-8} Torr, and substrate was inserted from a load lock chamber to maintain a low base pressure. A KrF excimer laser ($\lambda=248$ nm) was used for ablation of target. The laser power density and repetition frequency were 250 mJ/cm^2 and 5 Hz , respectively. The P_{O_2} was changed from 1 to 50 mTorr. The T_s was changed from 600 to 750°C . The film thickness was approximately 400 nm . In order to measure the electrical properties, the top Pt electrodes with a diameter of 0.2 mm were deposited on the film surface through a metal shadow mask by rf-magnetron sputtering.

The structural properties of the BNN thin films were characterized by XRD. The surface morphologies were observed by AFM. The electrical properties were measured by using the ferroelectric property measurement system RT-6000HVS manufactured by Radiant Technologies. The polarization-electric (P - E) hysteresis loops were measured using one-shot triangular waveforms with period of 50 ns .

3. RESULTS AND DISCUSSION

Figure 2(a) shows the XRD patterns as a function of T_s in BNN thin films. The P_{O_2} was fixed at 10 mTorr . The (100) and (200) of $\text{La}_{0.05}\text{Sr}_{0.95}\text{TiO}_3$ substrate peaks are observed at $2\theta=22.8^\circ$ and 46.5° , respectively. The (002) and (004) of the BNN thin films are observed at $2\theta=22.2^\circ$ and 45.3° , respectively. The (350) peak of the BNN thin film is also observed at $2\theta=29.5^\circ$. The BNN thin films prepared at $T_s=650$ and 600°C do not exhibit the existences of (002), (004) and (350) peaks, since the BNN thin films were not crystallized at the low T_s below 700°C . The existence of BaNb_2O_6 phase do not observed.

Figure 2(b) shows the intensities of (350) and (004) estimated from Fig.2 (a). The bottom axis represents the T_s . The estimations of the intensities are normalized by $\text{La}_{0.05}\text{Sr}_{0.95}\text{TiO}_3$ substrate peaks. The intensity of (004) peak increases slightly at $T_s \leq 700^\circ\text{C}$ and decreases above $T_s > 750^\circ\text{C}$. The intensity of (350) peak increases with increasing T_s . These behaviors are considered to be due to the amount of oxygen vacancy with high T_s .

Figure 3(a) shows the XRD patterns as a function of P_{O_2} in BNN thin films. The T_s was fixed at 700°C . The (002) and (004) of the BNN thin films are observed at $2\theta=22.2^\circ$ and 45.3° , respectively. Closed circle indicates the BaNb_2O_6 . The existence of (350) peak is observed at $2\theta \sim 29.6^\circ$ in these BNN thin films. The existence of BaNb_2O_6 phase is observed at $P_{\text{O}_2}=50 \text{ mTorr}$.

Figure 3(b) shows the intensities of (350) and (004) estimated from Fig.3 (a). The bottom axis represents the log scale P_{O_2} . The estimations of the intensities are normalized by $\text{La}_{0.05}\text{Sr}_{0.95}\text{TiO}_3$ substrate peaks. Although the intensity of (004) peak does not depend on $P_{\text{O}_2} \leq 10 \text{ mTorr}$, that decreases at $P_{\text{O}_2} > 10 \text{ mTorr}$. The intensity of (350) peak increases with increasing P_{O_2} . From Figs. 2 and 3, one can find that the BNN thin film at $P_{\text{O}_2}=7.5 \text{ mTorr}$ exhibits a highly *c*-axis orientation.

The P_{O_2} of the highly *c*-axis oriented BNN thin film accords with that of BNN thin film on MgO substrate prepared by Masuda *et al* [10]. The P_{O_2} dependence of BNN thin film might be closely related with the substrate temperature since the amount of oxygen vacancy in the thin film depend on the substrate temperature, as shown in Fig. 2.

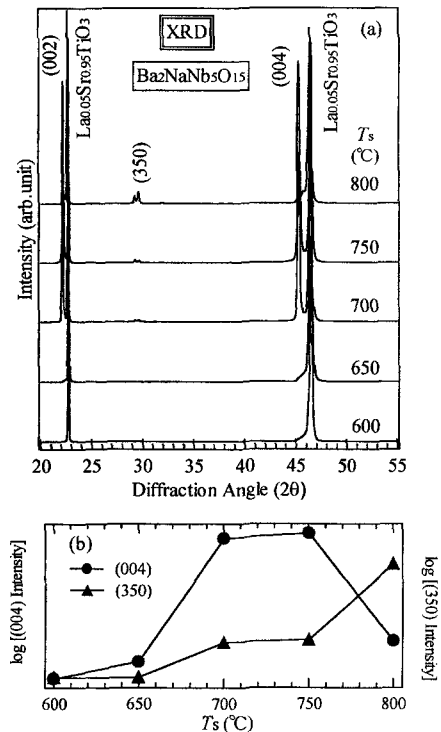


Fig. 2 (a) XRD patterns as a function of T_s in BNN thin films. (b) Intensities of (004) and (350) peaks

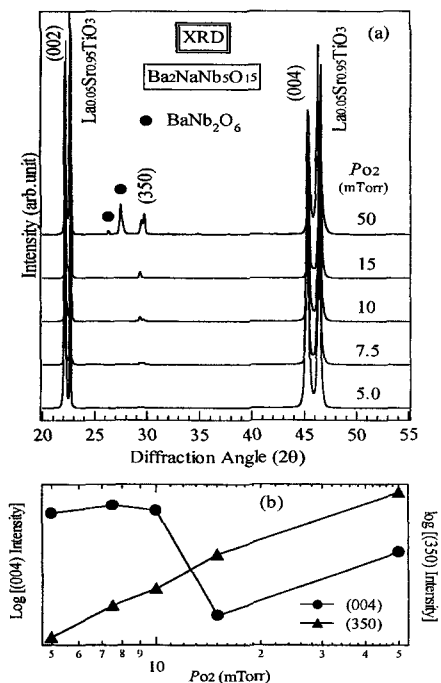


Fig. 3 (a) XRD patterns as a function of P_{O_2} in BNN thin films. (b) Intensities of (004) and (350) peaks.

Figure 4 shows the AFM image of the highly *c*-axis oriented BNN thin film prepared at $P_{O_2}=7.5$ mTorr and $T_s=700$ °C. The highly *c*-axis oriented BNN thin films consisted of well-developed grains with diameter of around 100 nm. The surface roughness R_{ms} was approximately 15 nm against the film thickness of 400 nm.

Figure 5 shows the surface roughness and grain size as a function of P_{O_2} . The surface roughness increases with increasing P_{O_2} . The grain size does not change with increasing P_{O_2} . The grain size does not change $P_{O_2} < 10$ mTorr and increases $P_{O_2} > 10$ mTorr. In particular, the grain size at $P_{O_2} > 15$ mTorr equals to the film thickness or surface roughness. The bad surface smoothness and large grain size at $P_{O_2} > 15$ mTorr might be explained as follows. The particles ablated from the target migrate on the heated substrate and form crystal nuclei at steps or kinks on the substrate due to the large interface energy between the BNN thin film and the substrate. Therefore, three-dimensional island-like crystal growth occurs [15].

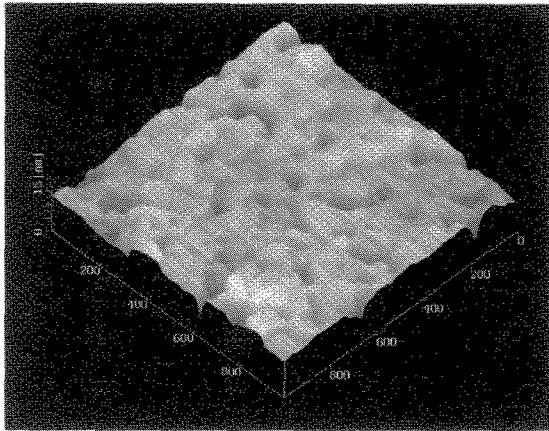


Fig. 4 AFM images of highly *c*-axis oriented BNN thin films deposited at $P_{O_2}=7.5$ mTorr and $T_s=700$ °C.

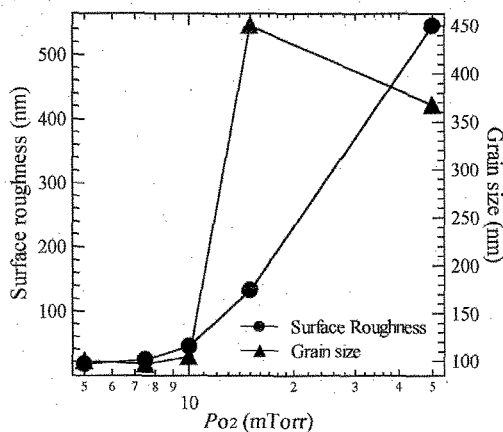


Fig. 5 Surface roughness and grain size as a function of P_{O_2} .

Figure 6(a) shows the hysteresis loops of the highly *c*-axis oriented BNN thin film. The as-deposited BNN thin film did not exhibit the ferroelectricity. Therefore, the BNN thin film was annealed at 700 °C in oxygen atmosphere for 1h in order to investigate the effect of

postannealing. The leakage current was improved from $\sim 10^{-3}$ A/cm² to $\sim 10^{-6}$ A/cm² by the postannealing. The both $2P_r$ and $2E_c$ values increase rather steeply at a low applied voltage but do not change much beyond 20 V, as shown in Fig. 5(b). The loop is nearly saturated at an applied voltage of 25 V and showed a unique fat shape. Then, the $2P_r$ and $2E_c$ were estimated to be 95.3 $\mu\text{C}/\text{cm}^2$ and 400 kV/cm, respectively. The dielectric constant (ϵ) was about 900 at room temperature. Although the effect of leakage current is included in the BNN thin film, these values are superior to those of the BNN thin films prepared by rf-magnetron sputtering and sol-gel method [9-12]. However, the above results are not sufficient for application to ferroelectric memory device since the ϵ of the BNN thin film is 18 times as large as that of BNN single crystal [1,2,15]. The large ϵ might be due to large grain size (~ 100 nm), as shown in Fig. 4(a).

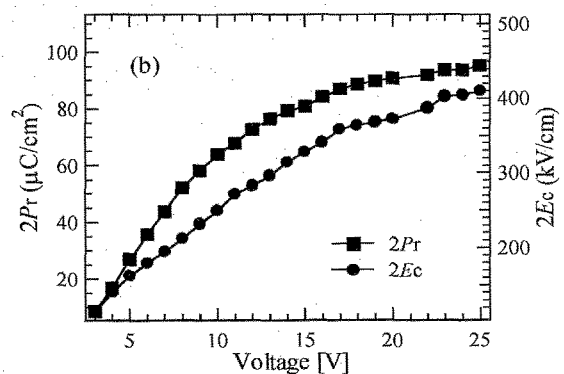
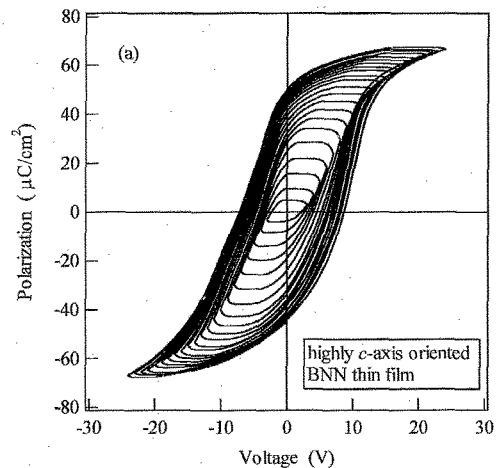


Fig. 6 (a) P - E hysteresis loops of highly *c*-axis oriented BNN thin film deposited at $P_{O_2}=7.5$ mTorr. (b) P_r and E_c as a function of voltage in highly *c*-axis oriented BNN thin film deposited at $P_{O_2}=7.5$ mTorr.

4. CONCLUSION

In conclusion, we prepared the highly *c*-axis oriented BNN thin film on $\text{La}_{0.05}\text{Sr}_{0.95}\text{TiO}_3$ substrate by PLD method. The structural properties of BNN thin films were dependent on P_{O_2} and T_s during deposition. When the P_{O_2} and T_s were fixed at 7.5 mTorr and 700

°C, respectively, the BNN thin film exhibited a highly c-axis oriented BNN single phase. The c-axis oriented BNN thin film consisted of well-developed grains and exhibited a good P - E hysteresis loop. Then, P_r and E_c were $2P_r=95.3 \mu\text{C}/\text{cm}^2$ and $2E_c=400 \text{ kV}/\text{cm}$, respectively, although the effect of leakage current was included. To further investigate the electrical properties of the BNN thin films, it is necessary to perform a more systematic optimization of the deposition and the postannealing conditions of the BNN thin films.

ACKNOWLEDGEMENTS

We would like to thank Prof. Y. Masuda and Ms. M. Takayasu for their useful discussions. This work was partially supported by the Foundation for Materials Science and Technology of Japan (MST Foundation), and the Grant-In-Aid for Scientific Research from the Ministry of Education, Cultures, Sports, Science and Technology.

REFERENCES

- [1] F. R. Nash, E. H. Turner, P. M. Bridenbaugh and J. M. Dziedzic: *J. Appl. Phys.* **42** (1972) 1.
- [2] E. A. Giess, B. A. Scott, G. Burns, D. F. Okane and A. Segmüller: *J. Am. Ceram. Soc.* **52** (1969) 276.
- [3] E. A. Giess, G. Berns, D. F. Okane and A. W. Smith: *Appl. Phys. Lett.* **11** (1967) 233.
- [4] J. E. Geusic, H. J. Levinstein, S. Singh, R. G. Smith and L. G. Van Uitert: *Appl. Phys. Lett.* **12** (1968) 306.
- [5] P. B. Jamieson, S. C. Abrahams and J. L. Bernstein: *J. Chem. Phys.* **48** (1968) 5048.
- [6] S. H. Wemple and M. DiDomenico: *J. Appl. Phys.* **40** (1969) 735.
- [7] A. Agostinelli, G. H. Braunstein and T. N. Blanton: *Appl. Phys. Lett.* **63** (1993) 123.
- [8] L. S. Hung, J. A. Agostinelli and J. M. Mir: *Appl. Phys. Lett.* **62** (1993) 3071.
- [9] G. Fujihashi, A. Kakimi, S. Ando, S. Okamura, T. Tsuchiya and T. Tsukamoto: *J. Ceram. Soc. Jpn.* **105** (1997) 449.
- [10] Y. Masuda, H. Masumoto, A. Baba, T. Goto and T. Hirai: *Jpn. J. Appl. Phys.* **32** (1993) 4043.
- [11] Y. Masuda, H. Masumoto, Y. Kidachi, A. Watadzul, A. Baba, T. Goto and T. Hirai: *Jpn. J. Appl. Phys.* **34** (1995) 5124.
- [12] Y. Masuda, H. Masumoto, A. Baba, Y. Kidachi and T. Hirai: *Ferroelectrics* **195** (1997) 297.
- [13] D. Baba, T. Higuchi, H. Kakemoto, Y. Tokura, S. Shin and T. Tsukamoto: *Jpn. J. Appl. Phys.* **42** (2003) L837.
- [14] K. Ohnuki, T. Higuchi, M. Takayasu, M. Sogawa and T. Tsukamoto: *Proc. Inter. Symp. Appl. Ferro. (ISAF) XIII* (2002) 171.
- [15] M. Sogawa, T. Higuchi, T. Kamei and T. Tsukamoto: to be published in *Jpn. J. Appl. Phys.* **42** (2003).